AD-A274 803

CUMENTATION PAGE

Form Approved
OMB No. 0704-0188

ation is estimated to average 1 hour per response, including the time for reviewing instructions, searching existing data sources, pleting and reviewing the collection of information. Send comments regarding this burden estimate or any other aspect of this educing this burden, to Washington Headquarters Services, Directorate for Information Operations and Reports, 1215 Jefferson 2, and to the Office of Management and Budget, Paperwork Reduction Project (0704-0188), Washington, DC 20503.

2. REPORT DATE	3. REPORT TYPE AND DATES COVERED
January 1994	Scientific No. 2

4. TITLE AND SUBTITLE
CRRES High Energy Proton Flux Maps

5. FUNDING NUMBERS
PE 62101F
PR 7601 TA 22 WU BO

Contract F19628-92-K-0003

6. AUTHOR(S)
M. S. Gussenhoven*
E. G. Mullen*
M. D. Violet*
C. Hein**
J. Bass**
D. Madden

7. PERFORMING ORGANIZATION NAME(S) AND ADDRESS(ES)
Boston College
Institute for Space Research
Chestnut Hill, MA 02167

DTIC
ELECTE
JAN 21 1994
S E D

8. PERFORMING ORGANIZATION REPORT NUMBER

9. SPONSORING/MONITORING AGENCY NAME(S) AND ADDRESS(ES)
Phillips Laboratory
29 Randolph Road
Hanscom AFB, MA 01731-3010

Contract Manager: Michael Violet/GPSP

10. SPONSORING/MONITORING AGENCY REPORT NUMBER
PL-TR-94-2004

11. SUPPLEMENTARY NOTES * Phillips Lab, Hanscom AFB, MA 01731-3010; ** Radex Inc, Bedford, MA 01730

Reprinted from IEEE Transactions on Nuclear Science, December 1993

12a. DISTRIBUTION/AVAILABILITY STATEMENT
Approved for public release; distribution unlimited

12b. DISTRIBUTION CODE

13. ABSTRACT *(Maximum 200 words)*

Proton flux maps of near-Earth space are presented using the Proton Telescope (PROTEL) detector on CRRES. The proton energy range covered is 1 - 100 MeV. Contamination of PROTEL measurements due to > 100 MeV protons is corrected using loss cone data, resulting on consistency with dosimeter measurements and a Monte Carlo computer model of PROTEL. Two states of the inner magnetosphere were found during the CRRES mission, a quiet state having a single proton belt, and an active state with a double belt. The properties of the new population in the second belt are presented. Comparisons with NASA proton codes are made.

14. SUBJECT TERMS
CRRES
High energy proton flux
Proton Telescope (PROTEL)

15. NUMBER OF PAGES
8

16. PRICE CODE

17. SECURITY CLASSIFICATION OF REPORT	18. SECURITY CLASSIFICATION OF THIS PAGE	19. SECURITY CLASSIFICATION OF ABSTRACT	20. LIMITATION OF ABSTRACT
Unclassified	Unclassified	Unclassified	SAR

Best
Available
Copy

PL-TR-94-2004

DTIC QUALITY INSPECTED 1

NTIS CRA&I
DTIC TAB
Unannounced
Justification
By
Distribution/
Availability Codes
Dist | Avail and/or Special
A-1

94-01796

CRRES High Energy Proton Flux Maps

M.S. Gussenhoven, E.G. Mullen, M.D. Violet
Phillips Laboratory, Geophysics Directorate,
Hanscom AFB, MA 01731

C. Hein, J. Bass
RADEX, Inc., Bedford, MA 01730

and

D. Madden
Boston College, Chestnut Hill, MA 02167

Abstract

Proton flux maps of near-Earth space are presented using the Proton Telescope (PROTEL) detector on CRRES. The proton energy range covered is 1 - 100 MeV. Contamination of PROTEL measurements due to > 100 MeV protons is corrected using loss cone data, resulting in consistency with dosimeter measurements and a Monte Carlo computer model of PROTEL. Two states of the inner magnetosphere were found during the CRRES mission, a quiet state having a single proton belt, and an active state with a double belt. The properties of the new population in the second belt are presented. Comparisons with NASA proton codes are made.

I. INTRODUCTION

The Combined Release and Radiation Effects Satellite (CRRES) hosted the most sophisticated complement of high energy particle detectors ever flown in the inner magnetosphere. It gathered data from July 1990 to October 1991 in a geosynchronous transfer orbit (perigee, 350 km; apogee 35000 km; orbital period 10 hr., inclination 18.2°). The CRRES data provide a unique opportunity to reassess existing radiation belt models and to study dynamic processes in the inner magnetosphere. To date, we have used the CRRES dosimeter data to evaluate the NASA radiation belt models using an undocumented transport code [1, and references therein], to create CRRES dose maps for quiet and active conditions [2], and to provide a personal computer utility to predict dose behind four different thicknesses of aluminum for an arbitrary satellite orbit for quiet and active CRRES conditions [3]. In addition, the CRRES high energy electron data have been used to model the variability of the outer zone electrons and to relate the variability to the magnetic index Ap [4]. In this paper we provide a summary of flux maps of the high energy (1-100 MeV) proton environment in the inner magnetosphere.

Particle flux, compared to dose, has more utility in the space community. Dose can only be directly measured behind a limited number of shielding shapes and thicknesses. Particle flux, on the other hand, if specified for a complete range of particle types, energies, and directions, can be used, with an accurate transport code, to calculate dose anywhere in any space structure. It is also needed by the biological community for manned space missions. Cell damage depends on particle type, energy and rate of exposure, as well as total exposure.

In this paper we: i) Describe the data base used to generate the flux maps including corrections for contamination by high energy penetrating particles in the inner belt. ii) Describe our flux map generation procedures and assumptions. iii) Show characteristics of the CRRES proton maps for quiet and active periods sampled during the CRRES mission. iv) Compare the quiet and active maps to the NASA proton model (AP8MAX) for solar maximum conditions.

II. DATA BASE

The instrument that we use to generate the CRRES proton flux maps for energies from 1 to 100 MeV is the Proton Telescope (PROTEL). PROTEL has two detector heads which, together, measure protons from 1 to 100 MeV in 24 energy steps. The angular resolution of the detector low (high) energy head is $\pm 10° \times \pm 10°$ ($\pm 12° \times \pm 17°$). A full description of PROTEL is available elsewhere [5, 6]. The PROTEL detectors are comprised of detector stacks and a logic system that requires single or double coincidence to verify that the proper energy particle is counted. In addition, both active and passive shielding are used around much of the detector stack. The detectors were extensively calibrated prior to launch. During calibration it was found that energetic protons (> 60 MeV) incident over a large angular range with respect to the detector axis could degrade sufficiently in the shielding, pass through the necessary angle in the detector stack and be counted. This contamination was found to be significant enough for very hard spectra to require correction.

To better understand the contamination of PROTEL from >60 MeV protons, a computer model of the instrument was created and a Monte Carlo ray tracing code devised [7] to provide the response function of PROTEL to protons with isotropic or mirror plane angular distributions and whose differential flux follows a power law (E^N) energy dependence, where N is negative. Results from the computer model, when

94 1 19 008

compared to calibration results, showed reasonable agreement with measured off-axis penetration. Almost all (>98%) of the contamination predicted by the computer model for the PROTEL response is contributed by protons with energy >100 MeV. To apply the results of the code as a correction method, it is first necessary to know the hardness (N in a power law description) of the >100 MeV proton spectrum and the angular distribution of this population for each L value (L designates the shell of magnetic field lines on which the particles are confined and is a measure, in Earth radii, R_E, of the magnetic equatorial distance of the shell). These parameters were not directly available on CRRES. Furthermore, the computer model correction varies with the orientation of the PROTEL detector with respect to the proton distribution in space (eg., the mirror plane). Thus, to be accurate, the corrections should be made on a second by second basis. This method is both computer intensive and hard to evaluate for correctness of application. For this reason we used a more physical approach.

The contamination of PROTEL can be seen most clearly when PROTEL is looking along the magnetic field direction, that is, into the loss cone. There should be no permanent population in the loss cone because these particles penetrate to the atmosphere where they are scattered (lost). If we assume that the loss cone is empty and that the contamination is independent of pitch angle, then it is reasonable to use the count rate in the first pitch angle bin just inside the loss cone as the background correction for those count rates outside the loss cone. The only remaining requirement is to determine the pitch angle at the edge of the loss cone. The maps made from the CRRES dosimeter data clearly determine, for each L-value, the maximum value of B/B_0 at which particles were measured. This value is easily converted to the equatorial pitch angle which is at the edge of the equatorial loss cone and is the value we apply to the PROTEL corrections. (It should be noted that in every case the equatorial loss cone determined in this manner was in agreement with the corresponding loss cone in the NASA AP8 models.)

A comparison of the correction made by assuming that the loss cone data represents the contamination from 100 MeV particles to that predicted by the computer model of PROTEL when the detector aperture is in the mirror plane is shown in Figure 1 for each energy channel in the high energy head. The percentages of contamination using the loss cone correction are average values taken from the PROTEL quiet model which is described below. Values at two L positions are shown in Figure 1, L = 1.25 R_E and 1.40 R_E. For determining the contamination from the PROTEL computer model we assumed that the > 100 MeV population had power law spectra with N of -1 and -2 for the two L-values, respectively. Considering that the two methods for making such a large correction are so different, the agreement is very good. The differences at low energy can be explained because no coincidence is used in the first two channels and they are subject to contamination from other than > 100 MeV protons. The loss cone correction for these two channels is > 100% for L = 1.25 R_E. This indicates a small pitch angle variation

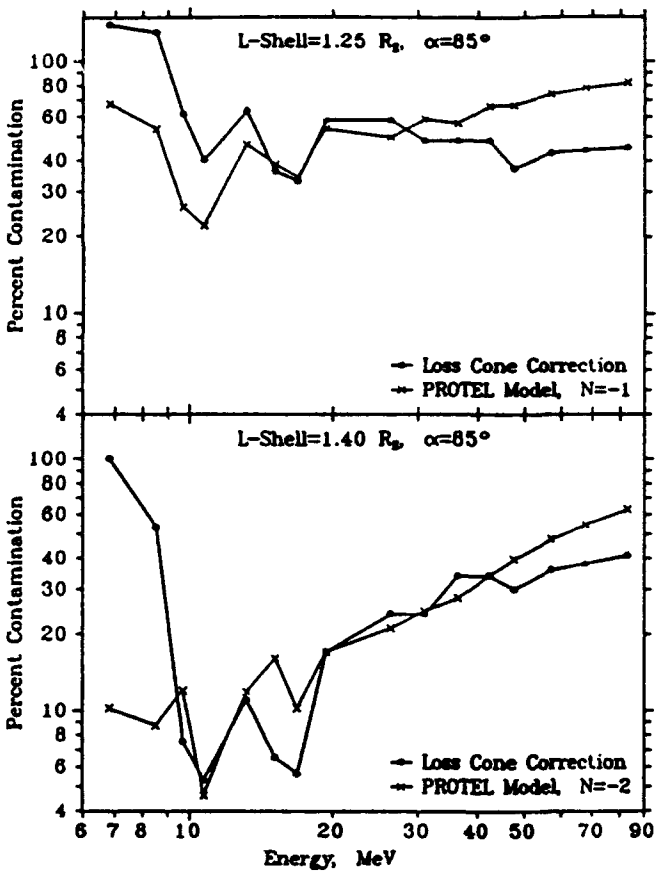

Figure 1. Comparison of estimates of percentage of contamination from the >100 MeV proton population for each PROTEL high energy head channel using the loss cone correction and the PROTEL computer model. The percentages are given for the detector pointing perpendicular to the magnetic field, and for two L-values: 1.2 R_E (top panel) and 1.4 R_E (bottom panel).

(assumed to be zero) in the contamination, which becomes significant when the actual counts are near background levels. At energies > 40 MeV there is a systematic divergence in the two methods that increases with decreasing L. For these energies the loss cone correction appears to be too small. However, for L = 1.4 R_E and greater, the difference is less than 20%. Considering the assumptions necessary to make the Monte Carlo model, we consider this an acceptable difference and therefore consider the model reliable above an L of 1.4 R_E. We note that at the L-value of 1.25 R_E, the correction using either method is large (from 40% to 80%) for energies > 50 MeV. It is questionable how much confidence can be placed in measurements that require up to an 80% correction; therefore the L = 1.25 data are considered suspect. Since the contamination falls off rapidly with increasing L beyond 1.4 R_E due to an overall softening of the proton spectrum, the data are brought into question over only a small (but important) region in L, eg., L < 1.4 R_E. From L = 1.4 - 2 R_E the loss cone and computer code methods of correction are in acceptable agreement, after which the >100 MeV proton population is too small to affect the lower energy measurements. However, application of the loss cone

correction is applied at all L values.

We summarize the difficulties we anticipate in modelling the high energy proton fluxes using the CRRES orbit and the PROTEL as follows: a) Wherever the proton population with energy >100 MeV falls off more slowly than E^{-2}, the loss cone correction is inadequate, and the contamination is as large as or greater than the measured population. The region where L is less than 1.4 R_E is such a region. b) The CRRES satellite traverses perigee so quickly that the temporal and pitch angle resolution of PROTEL is compromised. Thus, PROTEL cannot resolve the sharp fall-off of the inner edge of the radiation belt even if not subject to contamination there. The strength of the PROTEL modelling effort will be for L-values greater than 1.4 R_E, on and near the magnetic equator. Many of the low L ($L < 1.7\ R_E$) modelling issues have been previously addressed by observations made with low altitude satellites [8, 9] and with modelling efforts [10 and references therein].

III. Flux Maps And Models

The NASA radiation belt models are given in terms of particle omnidirectional integral flux at specific L and B/B_0 values (B/B_0 is the ratio of the magnetic field magnitude to the value on the same field line at the magnetic equator). The structure and parameters of the NASA models were chosen, in part, because of the limited computer memory and speed available at the time. Because we have more computing resources today, our models will be in terms of directional differential flux on the magnetic equator, as a function of L and pitch angle, α. We use the measured magnetic field to determine α and a model magnetic field to calculate L. The model field used combines the IGRF85 internal model [11] extrapolated to the time of measurement with the Olson-Pfitzer quiet external model [12]. If the full pitch angle distribution is specified on the magnetic equator, it can be projected along the magnetic field line to give the distribution anywhere on the field line. Thus, we can easily convert the average values in our maps to values in the AP8MAX grid, and vice versa.

The method of creating the proton flux maps is as follows:

i. Choose the sequence of orbits to be used for a particular model.

ii. Make any timing and look angle corrections and noise spike deletions required on the original data base.

iii. Map the data, point by point, to the magnetic equator using the model magnetic field Assign the proper L, B and α on the equator. (Note that the mapping of L is pitch angle dependent. The correction of the L value for pitch angle is only important for large L-values, eg. > 5 R_E.)

iv. Bin the data in pitch angle (18 - 5° degree bins) and L (180 - 1/20th R_E bins) maintaining separate files for the outgoing and ingoing legs of each orbit. Calculate each bin average and the bin average standard deviations for each leg of each orbit. Calculate an average standard deviation for each bin using all orbits for a given model. Reexamine the bin averages for each leg of each orbit, eliminating any individual bin average that is outside two standard deviations for that bin. On average the amount of data deleted in this manner ran between 2% and 4% per orbit. The exceptions were during moderate and large solar proton events. These events occur rarely enough that the fluxes at L values of 4 and greater during solar proton events lie outside the 2 sigma requirement. By deleting these cases, the proton maps, unlike the dose maps, represent only the populations of the inner magnetosphere.

v. For a given L-value identify the bin that is just inside the loss cone (for each leg of each orbit) and use the average flux value in this bin as background to be subtracted from all remaining bins of higher pitch angle at that L-value. Discard data in all bins of lower pitch angle, eg. well within the loss cone.

vi. Merge the individual legs and orbits to create for each L-bin and for each pitch angle bin outside the loss cone an average flux with an average standard deviation.

The collection of corrected average values, differential flux and standard deviation, constitutes the CRRES proton flux map for the sequence of orbits chosen.

High energy radiation belt protons have been thought to be extremely stable. The CRRES data have shown that major changes can occur in the belts when the magnetosphere is subject to an extremely intense solar wind shock front while a solar proton event is in progress. One such event occurred in March 1991, and this event has served as a dividing point for the dose maps [2, 13]. Prior to the event a single ("quiet") proton belt existed (over approximately 8 months). After the event, a double ("active") belt structure existed throughout the remainder of the CRRES lifetime (6 months). We similarly structure the proton flux maps. The quiet proton maps are constructed from PROTEL data taken during orbits 50 to 575 (15 Aug 1990 to 18 Mar 1991). Data taken during the first 49 orbits were not used because the magnetometer booms were in the process of deployment. A model field could have been used to estimate pitch angle, but we opted not to mix binning procedures. The active proton maps are constructed from PROTEL data taken during orbits 607-1067 (31 Mar 1991 to 11 Oct 1991).

The quiet and the active proton maps each consist of an array of 77760 average differential flux values accompanied by the same size array of average standard deviations. These arrays allow the full specification of the proton spectrum in the magnetic equatorial plane, in energy, from 1 - 100 MeV, and in pitch angle, from the loss cone to 90° for a given L value. To simplify the presentation of the maps, we model the pitch angle variation analytically, as has been commonly done in the past, by fitting it to the functional form, $\sin^n\alpha$ [8,10]. There is a very high correlation coefficient (0.9 to 1) between log flux and log $\sin\alpha$ whenever the particle flux is well above background levels. A notable exception to this occurs in the active model and is discussed below. For the most part then, the presentations that we make here will be in terms of the differential flux on the magnetic equator with pitch angle in the 85° bin (this pitch angle bin has a substantially larger data base than the 90° bin) and the power, n, of $\sin\alpha$ that

represents the pitch angle distribution. We present these numbers for representative energy channels covering the range of the detector.

A. *Differential Flux Profiles*

Figure 2 shows proton differential flux profiles in L on the magnetic equator. Four energies are used: 4.3±0.4, 9.7±0.4, 26.3±0.8 and 57.0±4.0 MeV in two pitch angle ranges: 85±2.5° (45±2.5°) in the set of panels on the left (right). Data for three models are displayed. The top panel gives values from the CRRES quiet maps, the middle panel from the CRRES active maps and the bottom panel from the NASA AP8MAX model. The profiles are shown out to an L-value of 4 R_E, by which point all but the lowest energy profile have reached background levels.

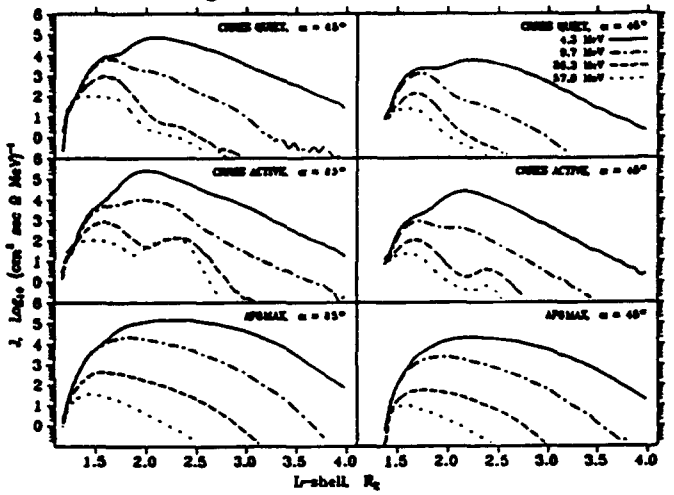

Figure 2. Differential flux profiles in L for three models: the CRRES quiet map (top), the CRRES active map (middle), and AP8MAX (bottom). Profiles for proton flux at two pitch angles on the magnetic equator are given: 85° (left) and 45° (right). Profiles for four energies are given in each panel as identified in the legend.

There are two major observations to be made from the flux profiles. The first is that the CRRES maps show that the region beyond L = 2 R_E is a dynamic one at all energies shown. The second is that the CRRES maps, while in reasonable agreement with AP8MAX in terms of overall flux intensity, show much more detailed structure which may be useful in identifying proton source, transport and loss processes. These observations hold not only for particles mirroring near the equatorial plane (85° pitch angle), but also for those mirroring well off the equator (45° pitch angle).

We first note the similarities in the profiles shown in Figure 2. The flux profiles from the CRRES proton maps and the AP8MAX model all show, for a given pitch angle, that the proton flux rises rapidly from a common origin [L = 1.15 (1.35) R_E, for pitch angle 85 (45)°]. All show that there is a systematic dispersion with energy in the flux peak of the profiles, the highest energy fluxes having peaks at the lowest L values. All profiles show that the fall-off rate of flux intensity beyond the peak is much slower than the rate of rise on the inner edge. And the models all show significant decreases in flux at all L-values between the 85° pitch angle profiles and those of 45° pitch angle. The peak flux values generally compare well, the CRRES values being somewhat higher than AP8MAX for the higher energies. For the most part the AP8MAX profiles fall more slowly than the CRRES quiet proton maps and thus, appear comparatively inflated above L = 2.5 R_E. However, they are not inflated enough to account for the dynamic increases at certain high energies for L values between 2 and 3 R_E in the active CRRES map. In general, we find the differences between the AP8MAX model and the CRRES proton maps to be sufficiently complex and subtle to explain the overall accuracy of AP8MAX in predicting proton dose for the CRRES orbit [1]. Clearly, there are orbits and periods of time for which the differences would not be small or subtle.

We now look at the dynamics of the outer edge of the radiation belt apparent in a comparison of the quiet and active CRRES maps. The difference between the two maps occurs almost entirely beyond L = 1.6 R_E. For the 85° pitch angle profiles all energies show large (up to two orders of magnitude) increases in flux compared to the quiet map fluxes from L=1.8 R_E outward. The increases are functions of pitch angle, energy and L-value. In L, the increases maximize between 2 and 3 R_E, and, in general, maximize at lower L-values for lower energies. In pitch angle, the increases maximize near 90°, although the confinement to the magnetic equator weakens greatly with decreasing energy. In energy the greater comparative changes with respect to the quiet model occur at higher energies, although significant increases occur between L = 2 and 3 R_E for all energies. The 'new' population in the active models is sufficiently separated from the old population for the higher energies that we have referred, in the past [2,11], to the new population as a third radiation belt (the second belt being the outer electron belt). The new belt is important for several reasons: For certain, high energies, eg. 57 MeV in Figure 2, the flux at the peak of the new belt is as high or higher than that in the inner belt. The new belt occurs in a region which is expected from the NASA models (bottom panel) to be reasonably benign. Thus, the unexpected presence of a harsh radiation population can pose serious problems to spacecraft operations [13].

When we look at the quiet map profiles from the perspective of those of the active maps, the fluxes beyond L = 2 R_E appear to be a decayed remnant of the extra belt in the active map. That is, there remain features suggesting a double population: an inner static population, and an outer one that can change dramatically under the right circumstances. The circumstances of the change in the outer region and the source of its population is a much debated subject at this time. We will consider the particle spectra and pitch angle distributions with this topic in mind.

B. *Standard Deviations*

Before proceeding we briefly look at the size of the

standard deviations in the CRRES maps. Figure 3 shows the ratio of the average values of σ (the standard deviation) to the average flux value for which σ was calculated, as a function of L, for the four energy values shown in Figure 2. The ratios are shown over the L range 1-3 R_E. Over this range the ratios vary from .1 to 5. The ratios are relatively flat over the region from L = 1.4 to 2.25 R_E which encompasses the heart of the inner belt. The relative value of σ minimizes here, being between 10% and 30% of the flux average. These values of σ are extremely small for magnetospheric particle populations and indicate not only the high degree of stability in the particle population here, but the appropriateness of the ordering functions, L, α, and the magnetic field models, as well as that of the correction for contamination. Below L = 1.4 R_E the ratio rises sharply with decreasing L until σ is as large as, or somewhat exceeds the average flux value itself. As pointed out above, it is in this region that the loss cone correction is large but perhaps not large enough. The large relative value of σ is a measure of the uncertainty in the map values in this region. The ratio also increases continuously beyond L = 2.5 R_E, reaching and exceeding the average flux value. In general, this increase is to be expected when the flux average falls to background levels. However, for the low energy fluxes, which are still well above background and unaffected by contamination here, the increase is a measure of the dynamical nature of the outer edge of the inner radiation belt. This includes large deviations of the actual magnetic field from the model field and the consequent inaccuracies in the L calculation and pitch angle mappings.

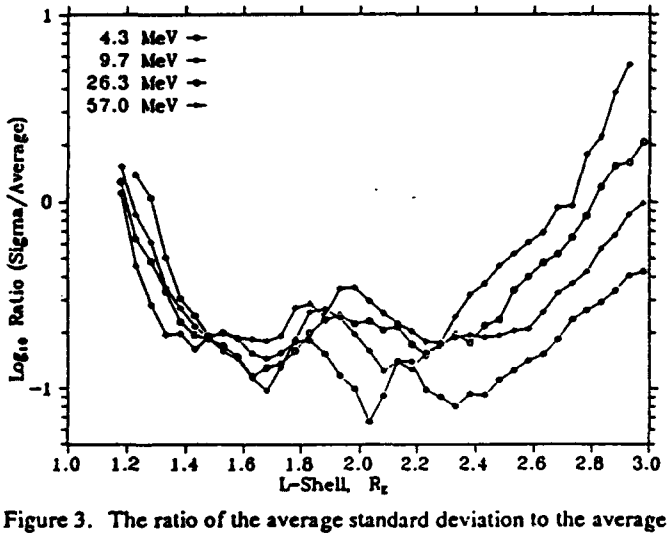

Figure 3. The ratio of the average standard deviation to the average flux value as a function of L for the active CRRES proton map. The ratios are for protons with pitch angle of 85° on the magnetic equator and having the four energies identified in the legend.

C. *Proton Differential Flux Spectra*

Figures 4 and 5 show a succession of proton differential flux spectra for increasing values of L taken from the CRRES proton maps. The differential flux in $(cm^2\ s\ sr\ MeV)^{-1}$ is plotted as a function of energy (in MeV). The energy scale is

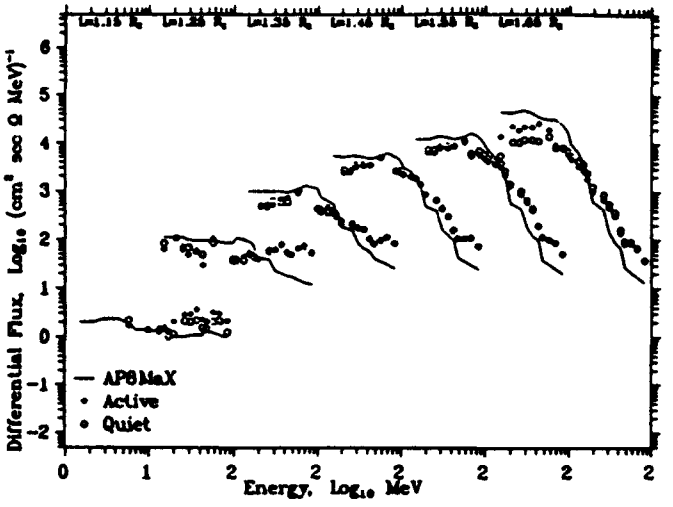

Figure 4. Differential flux as a function of energy at six L-values from 1.15 R_E to 1.65 R_E for protons with pitch angle of 85° on the magnetic equator. At each L-value three spectra are given. These are taken from the CRRES quiet map (open circles), the CRRES active map (solid diamonds) and AP8MAX (thin line). The spectra for each successive L-value are offset in energy by 1 decade from the previous one.

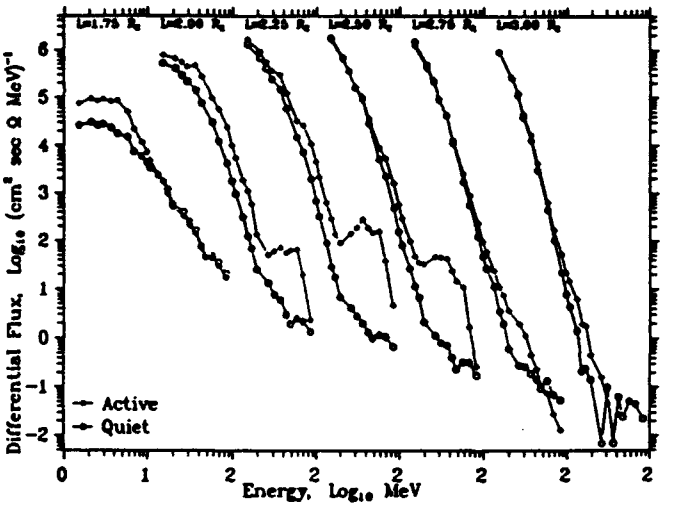

Figure 5. Differential flux as a function of energy at six L-values from 1.75 R_E to 3.00 R_E for protons with pitch angle of 85° on the magnetic equator. At each L-value two spectra are given. These are taken from the CRRES quiet map (open circles) and the CRRES active map (solid diamonds). The spectra for each successive L-value are offset in energy by 1 decade from the previous one.

incremented by one decade for each successive spectrum. The spectra are for protons with pitch angle of 85° on the magnetic equator. Flux values marked with open (closed) symbols are taken from the quiet (active) CRRES proton maps. In Figure 4, the corresponding spectra taken from AP8MAX are shown by thin solid lines. Spectra representing the inner belt (L-values from 1.15-1.65 R_E) are shown in Figure 4. Spectra representing protons in the second proton belt (L-values from 1.75-3.00 R_E) are shown in Figure 5.

In the inner belt, below L = 1.65 R_E, the CRRES spectra from the active and quiet periods are the same. (The differences in the values for the lowest L = 1.15 R_E are due to differences in the altitude sample of the two maps. This is also seen in the dose maps). Differences due to activity begin at L ~ 1.6 R_E in the low energy portion of the spectra. (See also Figure 5). There are, however, significant differences between the CRRES proton spectra and those of AP8MAX. For the two L-values < 1.3 R_E the CRRES proton spectra are flat or rising with increasing energy, while the AP8MAX spectra show a definite over-all decrease. There is some evidence in the literature that spectra of the kind shown in the CRRES maps occur at low L [10], but we suspect that inadequate correction for contamination from the >100 MeV population, as discussed above, leads to the spectral shapes shown here. The difference between the CRRES proton spectra and those of AP8MAX decrease somewhat with increasing L, but, in general, the CRRES spectra remain harder. Two factors contribute to this: the CRRES low energy fluxes are lower and the high energy fluxes higher than those of AP8MAX.

As we proceed outward in L in Figure 5 the differential flux spectra for the CRRES quiet period evolve from spectra peaked near 6 MeV (L = 1.35 R_E) to spectra peaked at lower and lower energies until the spectra are well-fit by a power law over the entire energy range from 1-100 MeV (ignoring noise at background levels). At L = 3.0 R_E the spectrum falls off as $E^{-6.5}$, an extremely soft spectrum.

For the active period the spectral changes with increasing L are much more complex. For L-values between 1.6 and 1.8 R_E there is a significant increase over the quiet period in fluxes below 10 MeV and no change at higher energies. By L = 2.0 R_E all energies show an increase in flux, but the increase in the energy range 20-70 MeV is far greater than at lower and higher energies. By the L-value of 2.5 R_E the increases in the low energy population have died out while the high energy increases persist. Beyond this distance the high energy increases fade away, as well.

The difference spectra between the quiet and the active maps represent the particle population that was "added" to the inner magnetosphere to create the new belt. These are shown in Figure 6 in the same format as Figure 5.

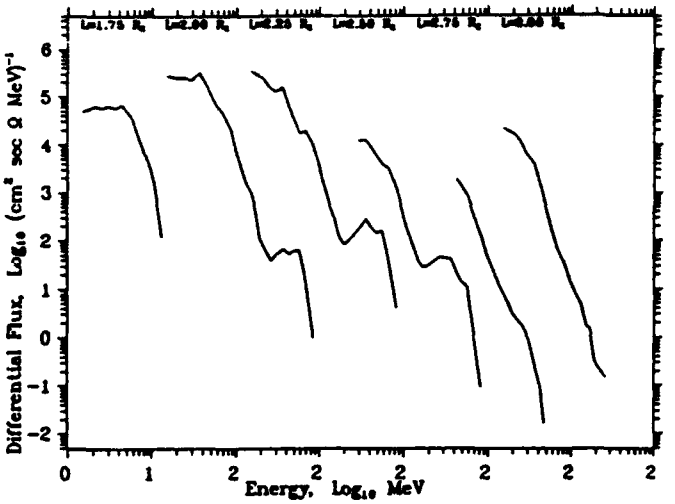

Figure 6. The proton differential flux that results from subtracting the CRRES quiet map values from the CRRES active map values shown in Figure 5, plotted as a function of energy. The spectra for each successive L-value are offset in energy by 1 decade from the previous one.

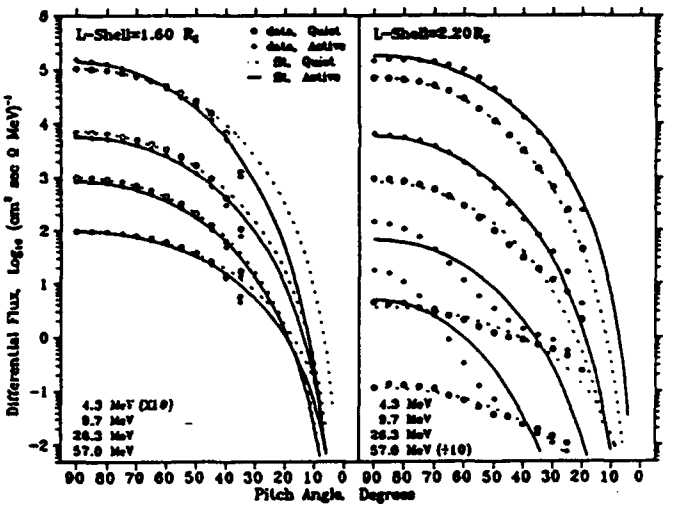

Figure 7. The proton differential flux plotted as a function of pitch angle for the four energies shown in the legend (decreasing flux levels are associated with higher energies). Measured values from the CRRES quiet (active) maps are represented by open circles (solid diamonds). Solid (dotted) lines represent best fits to the function $\sin^n\alpha$ (n determined by the fit). Two L-values are represented: 1.6 R_E (left panel) and 2.2 R_E (right panel).

D. Pitch Angle Distributions

To complete the specification of the proton environment one needs to know, in addition to the characteristics of the protons with pitch angle 85-90°, the variation of the differential flux with pitch angle. Figure 7 shows pitch angle distributions for the four representative energies used in Figure 2 for two values of L, 1.6 R_E in the left panel, representing the inner belt; and 2.2 R_E in the right panel representing the region of the new belt). The distributions for both quiet (open circles) and active (solid diamonds) models are superimposed. Dotted and solid lines show the $\sin^n\alpha$ fits to the distributions. In making the fits the flux values in the two lowest pitch angle bins were excluded. We discuss the two panels separately.

For the inner region, the $\sin^n\alpha$ fits to the distribution are excellent, excepting the excluded points. This generally holds throughout the inner belt whenever the flux levels are well above background. The two lowest pitch angle values that were excluded from the fits always fall off more rapidly than the functional value, indicating that pitch angle diffusion is operating near the loss cone. The pitch angle distributions for

the quiet and the active model are virtually identical. The fluxes peak strongly at 90°, n lying between 3 and 8, with the higher energies having the least strongly peaked distribution functions (eg., lowest values of n).

At L = 2.2 R_E, in the region of the new belt, the pitch angle distribution (right hand panel, Figure 7) indicates a more dynamic situation and $\sin^n\alpha$ fits to the distributions are not as uniformly good. They represent the lower energy populations best. But even in the 4.3 MeV population the pitch angle distributions show some differences compared to those in the inner belt. The pitch angles closest to the loss cone are not eroded, as in the inner belt, possibly indicating a 'younger' population. Of greater interest are the pitch angle distributions for the higher energy protons. First note that the distributions for the active period are not single $\sin^n\alpha$ distributions, but appear to be the sum of two such distributions, one equal to that of the quiet period, and a new, added one, much more strongly peaked and having greater intensity at 90°. Thus, in keeping with the 'added' population evident in the 90° energy spectrum, it appears that the added population retains its own pitch angle identity as well. One curious feature of the distributions in this region is that the double distribution is apparent even in the quiet period for the three highest energies, even though it is very weak.

Finally we compare the pitch angle distributions in the CRRES proton models to those of AP8MAX and to those that can be deduced from the B/B_0 variation in the CRRES dosimeter maps [2]. We use the parameter n, assuming $\sin^n\alpha$ fits to the pitch angle distributions for the comparison. Values of n are shown in Figure 8 for 36.3 MeV protons, and for the quiet (top) and active (bottom) dose and proton maps. We chose the 36.3 MeV PROTEL channel because this energy best fits one of the four thresholds of the dosimeter, 35 MeV. The overall agreement between model values of n is good except in the region of the new belt (active map, L > 1.9 R_E). After falling steeply from very high values at the lowest L, n flattens out for L between 1.3 and 1.6 R_E, and then slowly decreases, reaching a minimum at L ~2 R_E. There are systematic differences between the models at the lowest L values. The values of n deduced from the dosimeter maps are the highest and those of the CRRES proton maps the lowest. The reason for either of these is not transparent. However, the loss cone is so wide at low L that only a few points go into determining the $\sin^n\alpha$ fit.

Near L ~ 2 R_E and beyond the models show the greatest divergence, both in trend and in magnitude. AP8MAX is nearly featureless here, while the CRRES maps show considerable variation in L and in activity. In the quiet models, both the CRRES dosimeter and PROTEL models show a clear minimum in n at ~ 2 R_E which is not shown in AP8MAX. The protons are most isotropic here even though in the quiet period the fluxes are very low. In the active model, the minimum is "interrupted" by the new belt population which is much more strongly peaked, as discussed above, near 90°. The dosimeter and PROTEL show remarkable agreement in the $\sin^n\alpha$ fits from L = 2.0-2.5 MeV, indicating that the pitch angle distribution is not

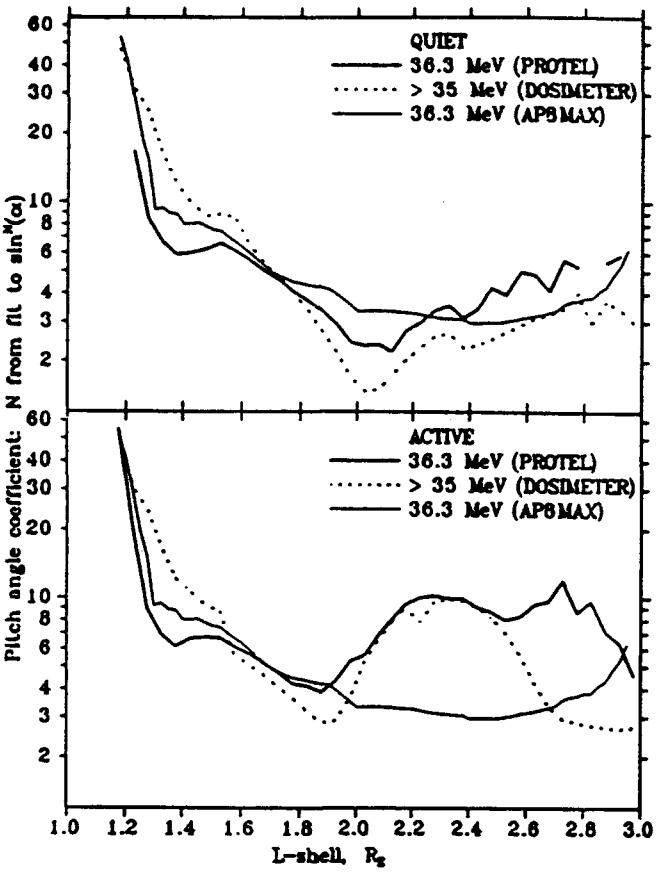

Figure 8. The pitch angle coefficient, n, resulting from $\sin^n\alpha$ fits to the 36 MeV proton pitch angle distributions, plotted as a function of L. Values are shown for CRRES quiet (top panel) and active (bottom panel) conditions and for AP8MAX (thin line in both panels). Values from two CRRES instruments are represented: PROTEL (thick line) and the Space Radiation Dosimeter (dotted line).

strongly energy dependent (recall that the dosimeter measurement is integral in energy) and/or the proton population in the new belt falls off rapidly beyond 35 MeV, which we have shown above to be the case. The reason that the two disagree strongly above L = 2.5 is not clear. We speculate that the very high electron population that accompanied the second proton belt may affect the dosimeter results. It is not known at this time how confined to the equator this population is. Recall too, that beyond L = 2.5 the high energy proton population is rapidly decreasing.

The variations of the pitch angle distributions with L, as do the variations of the proton population with energy discussed above, support the view that high energy protons in the inner magnetosphere populate two different regions, a stable inner region found below L ~ 2 R_E and a dynamic region above L = 2 R_E. There is no consistent indication in the pitch angle variations that the outer belt diffuses inward to populate the inner region since the degree of confinement to the magnetic equator does not steadily increase inward. Instead, the inner and outer belts are separated by a region of increased isotropization.

IV. DISCUSSION

Accurate proton models are needed to design more reliable, autonomous and longer-lived space systems. The areas requiring improved models range from solar cell dose degradation, to EVA missions, to single event upset frequency. Shielding penalties can be enormous in both cost and capability. Particle directionality may be critical to space manufacturing. The CRRES dose models [2,3] were the first steps in replacing the NASA models with more accurate data bases. Many more are needed. This paper continues the process by constructing proton maps over the energy range 1 - 100 MeV for quiet and active conditions during solar maximum. In doing so we have been very critical of possible weaknesses in the PROTEL measurements and our ability to correct for high energy proton contamination. We feel that the CRRES proton maps have greatest accuracy for L values $> 1.4\ R_E$ and are questionable below this value. They have greatest applicability for dynamical changes that can occur at the outer edges of the stable inner belt.

The major finding in the CRRES maps is that there appear to be two quite distinct regions in the inner magnetosphere which are populated by high energy protons. One is a stable inner region existing at L-values below $1.8\ R_E$. Few changes in the proton population were found in this region over the CRRES lifetime, and the changes that were measured occurred for lower energies on the outer fringes of the region. The characteristics of the protons in this region have been quite successfully modelled [10] by assuming two sources: cosmic ray albedo neutron decay (CRAND) and the population on the $1.8\ R_E$ boundary that diffuses inward. It is well-known that this proton population is increasingly confined to the magnetic equator and has an increasingly harder (more energetic) spectrum with decreasing L, and the CRRES results also show this.

Beyond an L-value of $1.8\ R_E$ the CRRES measurements revealed a proton population that cannot be treated as a continuous extrapolation of the inner population, as is found in AP8MAX. A new population can exist here, brought in under extreme solar wind conditions. Characteristics of the new population show that it is apparently simply added to the pre-existing population. The added population is strongly confined to the equatorial plane and is strongly peaked in energy at about 35 MeV. In fact, the population is so strongly peaked in energy that it should be unstable, and erode itself through wave generation. This does not happen. The population remains and is essentially unchanged for many months from its creation to the end of the CRRES mission. During this time the region with L-values from $2 - 3\ R_E$ presents a radiation hazard that is not modelled by AP8MAX.

AP8MAX may well be a compromise, or average, between the two states measured by CRRES. Presumably, incidents that add high energy protons to the region for $L > 1.8\ R_E$ occurred during the time AP8MAX data were gathered. The AP8MAX flux profiles in L indicate this. They show a smoothly varying single belt that has significant fluxes out to higher L values than measured in the quiet period on CRRES, and to lower L values than the active period. There are two obvious problems in such an average model. First, and more fundamentally, the average washes out information about the source, transport and loss processes for protons in the inner magnetosphere. Second, and more practically, it will greatly underestimate the radiation hazard for missions that spend a significant amount of time between L values of 1.8 and $3\ R_E$ during active periods.

The new proton maps presented here show significant variations from existing theory and models to warrant making a new assessment of the inner magnetosphere for design of near-Earth systems. Without new proton model specifications design lifetime predictions will not be reliable and optimum shielding levels will not be flown.

V. REFERENCES

[1] M.S. Gussenhoven. E.G. Mullen, D. H. Brautigam, E. Holeman, C. Jordan, F. Hanser and B. Dichter, "Preliminary comparison of dose measurements on CRRES to NASA model predictions", IEEE, Trans. Nucl.Sci., 38, 1655, 1991.

[2] M.S. Gussenhoven, E.G. Mullen, M. Sperry, K.J. Kerns and J.B. Blake, "The effect of the March 1991 storm on accumulated dose for selected satellite orbits: CRRES dose models", IEEE, Trans. Nucl.Sci., 39, 1765, 1992.

[3] K.J. Kerns and M.S. Gussenhoven, *"CRRESRAD Documentation*, PL-TR-92-2201, Phillips Laboratory, Hanscom AFB, MA, 1992.

[4] D.H. Brautigam, M.S. Gussenhoven, and E.G. Mullen, "Quasi-static model of outer zone electrons", IEEE, Trans. Nucl.Sci., 39, 1797, 1992.

[5] M.D. Violet, K. Lynch, R. Redus, K. Riehl, E. Boughan and C. Hein, "Proton telescope (PROTEL) on the CRRES spacecraft", IEEE, Trans. Nucl. Sci., 40, 242, 1992.

[6] K. Lynch, E. Boughan, D. Fischi, D. Hardy and K. Riehl, *"PROTEL: Design, Fabrication, Calibration, Testing and Satellite Integration of a Proton Telescope"*, AFGL-TR-89-0045, Air Force Geophysics Laboratory, Hanscom AFB, MA, 1989, ADA214564,

[7] C. Hein, private communication, 1992-1993.

[8] H. M. Fischer, V.W. Auschrat and G. Wibberenz, "Angular distribution and energy spectra of protons of energy $5 \leq E \leq 50$ MeV at the lower edge of the radiation belt in equatorial latitudes", J. Geophys. Res., 82, 537, 1977.

[9] R.S. White, "High energy proton radiation belt", Rev. Geophys. and Space Phys., 11, 595, 1973.

[10] V. Jentsch, "On the role of external and internal source in generating energy and pitch angle distributions of inner-zone protons", J. Geophys. Res., 86, 701, 1981.

[11] IAGA Division I Working Group, "International Geomagnetic Reference Revision 1985", EOS, Trans. Am. Geophys. U., 67, No. 24, 1986.

[12] W.P. Olson and K.A. Pfitzer, "A quantitative model of the magnetospheric magnetic field", J. Geophys. Res., 79, 3739, 1974.

[13] E.G. Mullen, M.S. Gussenhoven, K. Ray and M. Violet, "A double-peaked inner radiation belt: Cause and effect as seen on CRRES, IEEE, Trans. Nucl.Sci., 38, 1713, 1991.